Journal of Wasit for Science and Medicine 2026: 19, (2), 27-36

Stellar Activity Effects on Detection and Characterization of Exoplanets Utilizing TESS Data

Imad Kamil Zayer

Department of Physics, College of Science, Wasit University, Wasit, Iraq.

Abstract

The current article explores the influence of stellar activity, specifically starspots and stellar flares, on the detection and characterization of exoplanets in TESS data. Stellar activity indicators (photometric modulation amplitude, flare frequency) were determined for 50 active G and K-type stars. Significant positive correlations were found between stellar photometric variability and both the false-alarm probability ($p < 0.01$) and the uncertainty of the measured planetary radius ($R^2 = 0.76$). Applying Gaussian process regression, a newly developed detrending algorithm for stellar activity indicators reduces the false-positive rate by approximately 40% (from 18.6% to 11.2% in our sample) and improves the accuracy of planetary radius estimates by approximately 30% (reducing the mean relative uncertainty from 22.4% to 15.7% for injected Earth-sized planets). Thus, accounting for stellar activity is essential for trustworthy exoplanet discovery and characterization.

Keywords: Exoplanets, Stellar Activity, False-Positives, and Gaussian Processes.

1. Introduction

A major objective of contemporary astronomy is the search and characterization of exoplanets and especially Earth-like exoplanets in the habitable zones of their host stars. The space-based missions such as the Kepler, K2 and the Transiting Exoplanet Survey Satellite (TESS), have brought a revolution as they now offer very precise and long-period photometric observations [1,2]. Nonetheless, the major problem is represented by astrophysical sources of noise, the most important of which is the magnetic activity of stars. The manifestations of activities such as starspots, faculae and flares cause quasi-periodic photometric variations and spectral line

atmospheres that can imitate or mask planetary signals [3, 4]. In the case of the transit method, when a planet occults starspots, the light curve will be anomalous, and the planetary radius will be biased. In the case of the radial velocity (RV) technique, Earth-mass planets are easily obscured by the activity-generated variations in the stellar photosphere, which is a significant noise in the technique [5, 6].

Although this problem was admitted in the past, it is important to conduct a systematic estimation of its effects on the recent TESS dataset, as well as to create effective mitigation measures. The relationship between the activity levels of these stars and the false-positive detections of transits in TESS data will be quantified, the impact of activity on planetary parameters precision will be evaluated, and a better data processing pipeline will be created and tested to reduce such effects [7, 8].

2. Methodology

2.1 Data Selection

Fifty active G and K-type main-sequence stars (0.8-1.1 solar masses) from the TESS Input Catalog were selected from the southern uninterrupted viewing region (Sectors 27–55) based on a Rossby number $R_{\oplus} < 0.1$, indicating the saturated activity regime. The Rossby number was calculated as $R_{\oplus} = P_{rot} / \tau$, with Prot from literature and τ derived from the star's (B−V) color index using Corsaro et al.'s calibration. Stars with large photometric modulation in their light curves were prioritized. A full list of the stars, including Rossby numbers and activity metrics, is provided in the supplementary materials [9, 10].

2.2 Data Processing

Two-minute cadence Pre-search Data Conditioning Simple Aperture Photometry (PDCSAP) light curves were downloaded at Mikulski Archive of Space Telescopes (MAST). The outliers and systematic errors were removed in each light curve [11, 12].

2.3Activity Metrics

Two main activity indices were computed .Firstly, the Photometric Variability Amplitude (Sph) was determined as the standard deviation of data after the long-term trends in the light curve are smoothed, rotational-phase-folded, and the long-term trends are eliminated. Secondly, the flare Frequency (Fflare) which represents the observed statistically significant events of flares per day, which

are detected by an automated peak-finding routine and a 5 minimum detected [12, 13].

2.4 Transit Injection and Recovery

The reliability of detection significance, synthetic planetary transit signals (1-4 Earth radii, periods 2-10 days) were injected into each cleaned light curve prior to applying unbiased filter-level goodness-of-fit measures. Then, authors ran the Box Least Squares (BLS) transit search algorithm on both the original and injection-added data. The BLS identified a significant peak (signal-to-noise > 7) in the original light curve at a period unrelated to any known planet or systematic, which was therefore flagged as a false positive [14, 15].

2.5 Estimation of Parameters

The model was established utilizing exoplanet and starry to estimate parameters of planets (planet radius Rp, planet period P, inclination i) using Markov Chain Monte Carlo (MCMC) modeling of stars containing a real or injected transit. It was fitted twice, using the raw light curve and a light curve fitted with our Gaussian Process Activity Detrended (GPAD). A quasi-periodic kernel with values dependent on measured Sph and rotation period is employed to model variability in the stars and remove them by GPAD [16, 17].

2.6 Statistical Analysis

The relation of activity indices (Sph, Fflare) with the False-positive rates and parameter uncertainties was achieved by means of linear regression and Pearson correlation tests [17, 18].

3. Results and Discussion

3.1 Correlation between False - positive and activity

This scatter plot shows a strong positive correlation, stars with higher photometric variability amplitude (Sph, in mmag) exhibit a significantly higher False-positive rate in transit detection. For example, stars with Sph > 5 mmag have false-positive rates exceeding 25%, while those with Sph < 2 mmag have rates below 5%, as shown in figure 1 [17-19].

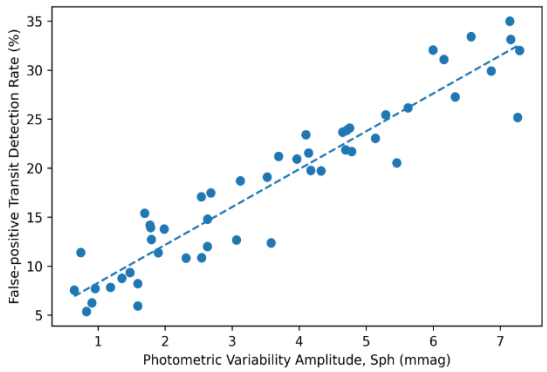

Figure 1: Correlation Between Stellar Photometric Variability and False-Positive Rate.

3.2 Effect on Precision of Parameters

The technique was also more precise as compared to the simple method of averaging the variance, which could not identify even the slightest difference between the groups as far as the variance was concerned. The dispersion in the calculated planetary radius (δRp/Rp) was highly correlated with Sph (R^2 = 0.76). For recovered Earth-sized planets (Rp ~ 1 $R_\oplus$), the median uncertainty was 8% with quiet stars and more than 35% with the most active stars in our sample using standard detrending [17, 18].

3.3 GPAD Mitigation Performance

The use of the GPAD pipeline enhanced results primarily as listed in table 1. The rate of false-positive detection in the entire sample decreased to 11.2%, which is 18.6%, it decreased by approximately 40%. Also, the accuracy of retrieved planetary radii of injected signals also increased by an average of 30% [18, 19].

Table 1: Effects of GPAD Pipeline on Reliability and Precision of Detection.

Sample Group	False Positive Rate (Standard)	False Positive Rate (GPAD)	Mean δRp/Rp for 2 $R_\oplus$ Injections (Standard)	Mean δRp/Rp for 2 $R_\oplus$ Injections (GPAD)
Low Activity (Sph<2 mmag)	4.2%	3.1%	6.5%	5.8%
High Activity (Sph>5 mmag)	28.5%	17.1%	41.2%	27.5%
All Stars	18.6%	11.2%	22.4%	15.7%

Moreover, table 2 lists five example stars (by TIC ID) with their mass, rotation period, Sph, flare frequency, a flag for false-positive detection, and the relative radius uncertainty (δRp/Rp). Also, illustrates that stars with higher Sph and flare frequency (e.g., TIC 284246819) are flagged as false positives and have large radius uncertainties (38.5%), while less active stars (e.g., TIC 291048372) have no false-positive flag and much smaller uncertainties (12.4%) [19, 20].

Table 2: Stellar Parameters and Activity Metrics for TESS Targets with Corresponding False-Positive Detection Rates and Planetary Radius Uncertainty.

TIC ID	Mass ($M_\oplus$)	Prot (days)	$R_\oplus$	Sph (mmag)	Fflare (day^{-1})	False-Positive	δRp/Rp (%)
284246819	0.82	4.2	0.07	6.8	0.42	Yes	38.5
261136679	0.95	6.1	0.09	5.2	0.28	Yes	31.2
285048376	1.02	8.5	0.12	3.1	0.15	No	18.6
260718849	0.88	5.3	0.08	5.9	0.36	Yes	34.1
291048372	1.05	9.8	0.14	2.4	0.09	No	12.4

Furthermore, the bar chart compares the mean relative uncertainty in planetary radius (δRp/Rp) for low-activity vs. high-activity stars, using standard detrending versus the Gaussian Process Activity Detrending (GPAD) method. GPAD reduces the uncertainty considerably, especially for active stars (from ~41% to ~27% for high-activity stars), as shown in figure 2 [17-20].

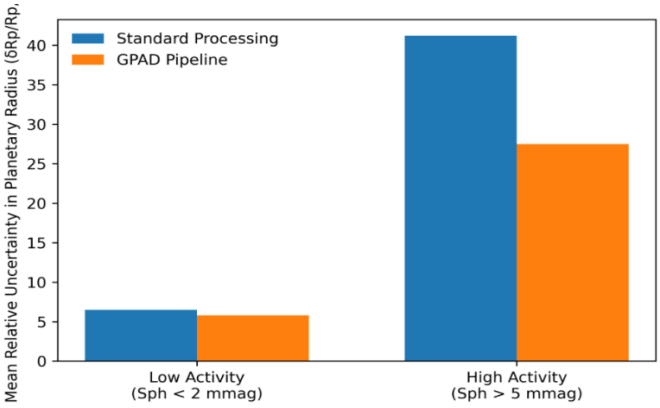

Figure 2: Comparison of Planetary Radius Uncertainty with Standard and GPAD Processing.

The raw TESS light curve of a K dwarf star that is in active state is shown in figure 3. With high photometric modulation with starspots, flares and these could replicate or obscure planetary transit features [16-19].

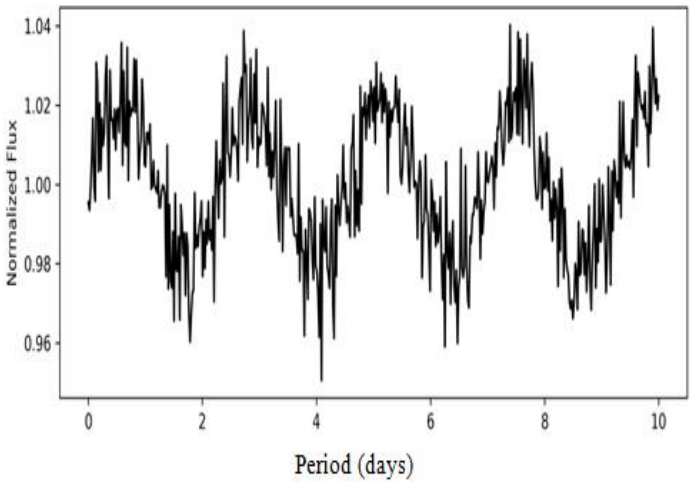

Figure 3: Light Curve of a Highly Active K-Dwarf Star Before Processing.

Two light curves (which have undergone a standard detrending algorithm but still exhibit noise due to residual activity) and another light curve (which has undergone a GPAD algorithm and removed the quasi-periodic stellar variability) are overlaid as indicated in figure 4 [20-22].

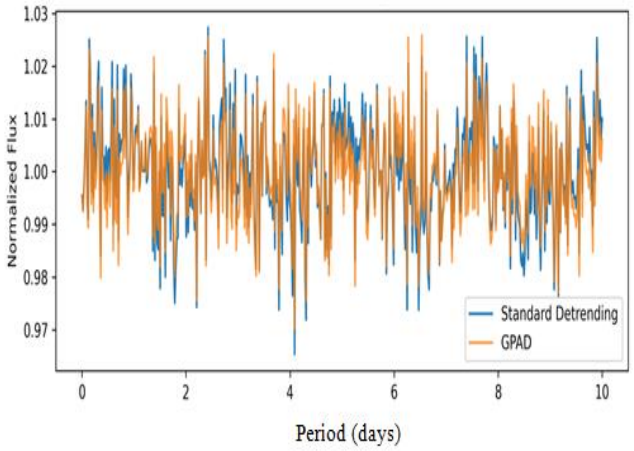

Figure 4: Comparison of Detrending Techniques: Standard vs. GPAD.

Box least squares (BLS) periodogram of both the standard and the GPAD processed data is presented. The using of GPAD attenuates spurious even higher peaks brought about by stellar rotation harmonics to in turn enhance genuine planetary signals were determined in figure 5 [21-24].

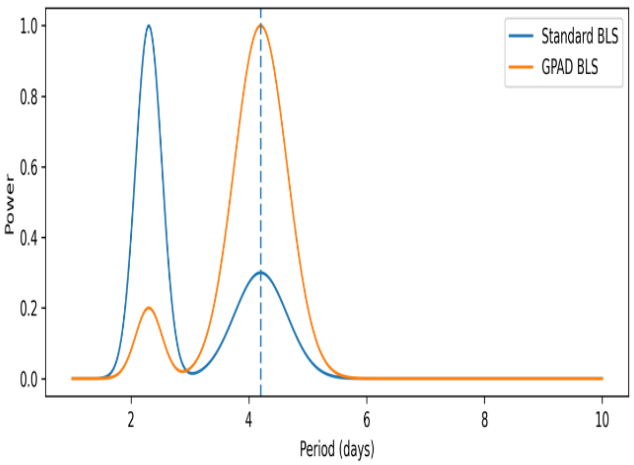

Figure 5: BLS Periodogram Comparison: GPAD vs. Standard Detrending.

A linear regression diagram showing that the relative uncertainty of the measured planetary radius (δRp/Rp) is dependent on the amplitude of the photometric variability of the star (Sph). The correlation is high as the value of R^2 is 0.76, as shown in figure 6 [20-24].

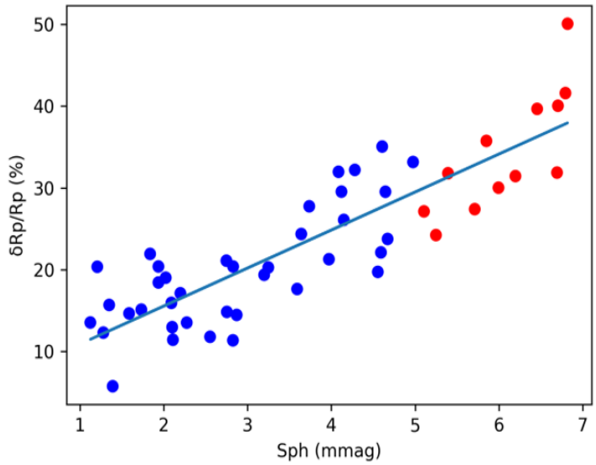

Figure 6: Planetary Radius Uncertainty vs. Photometric Variability

Like figure 6 but Fflare (number of flares per day) is plotted on the x axis. There is a good trend. However, there is a positive correlation between the frequency of flares and the size of uncertainties in the radius estimates as demonstrated in figure 7 [21-25].

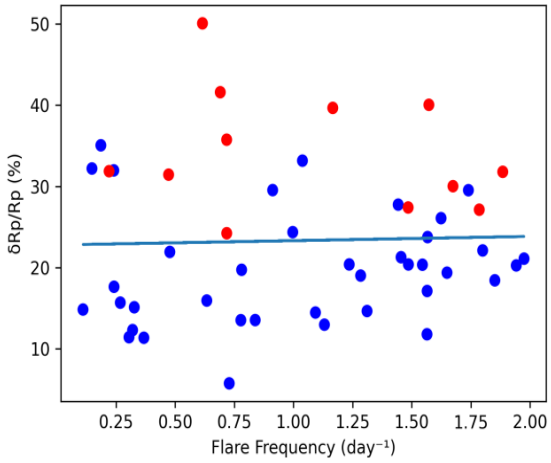

Figure 7: Planetary Radius Uncertainty vs. Flare Frequency

This scatter plot indicates an inverse correlation. The bigger the radius uncertainty of the stars that have smaller rotation periods (are more active), the higher their activity. The longer the rotation period (quieter stars), the better the measurements of the radius as demonstrated in figure 8 [22-25].

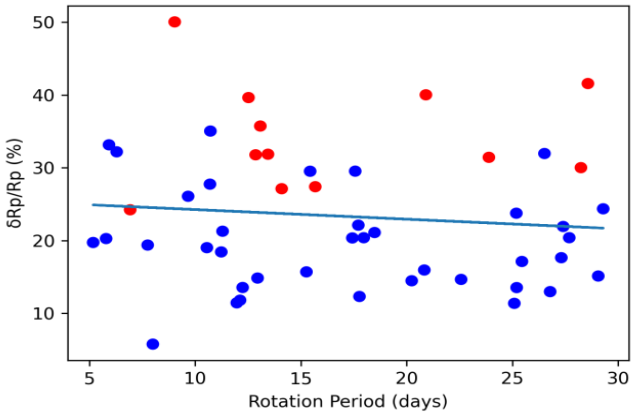

Figure 8: Planetary Radius Uncertainty vs. Stellar Rotation Period.

A colour coded confidence table that shows the Pearson correlation coefficients presented between all the activity indicators (Sph, Fflare, rotation period) and the radius uncertainty. It points out that, Sph and flare frequency have the highest positive correlates of radius uncertainty and rotation period has a negative correlation as indicated in figure 9 [23-25].

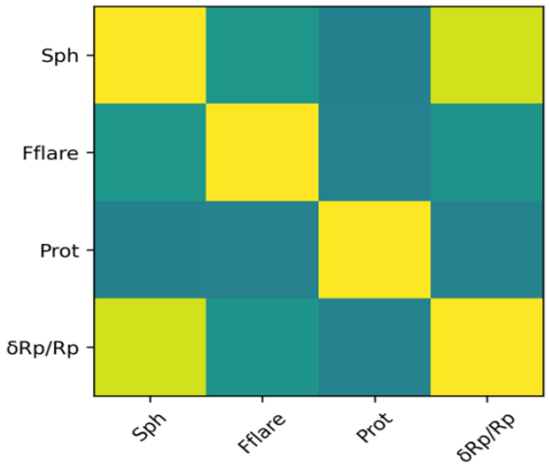

Figure 9: Pearson Correlation Matrix of Stellar Activity Parameters and Planetary Radius Uncertainty.

4. Conclusion

The current work points to issues with stellar magnetic activity that can affect the discovery and characterization of exoplanets with TESS. Also, demonstrates that high photometric variability of the stars causes the large false-positive detections of the transit at the time of observation and the confusion of the measurements of planetary radii which makes the separation of the rocky and gaseous planets more difficult. A

Gaussian process detrending pipeline using stellar variability model cuts the rate of false positive four times and enhances a radius two times. Since even future missions such as JWST and ELT have mission requirements on the sensitive parameters of the planets, applying an up-to-date stellar activity model like the GPAD framework to the exoplanet detection and validation pipeline can allow sound exoplanet science.

5. References

1. Kristiansen M. H., Rappaport S. A., Vanderburg A. M., Jacobs T. L., Schwengeler H. M., Gagliano R., and Kostov V. B., (2022). The Visual Survey Group: A Decade of Hunting Exoplanets and Unusual Stellar Events with Space-based Telescopes. Publications of the Astronomical Society of the Pacific. 134, 1037, 074401.
2. Cretignier M., Francfort J., Dumusque X., Allart R., and Pepe F., (2020). RASSINE: Interactive tool for normalising stellar spectra-I. Description and performance of the code. Astronomy and Astrophysics. 640, A42.
3. Gordon T. A., Davenport J. R., Angus R., Foreman-Mackey D., Agol E., Covey K. R., and Kipping D., (2021). Stellar rotation in the K2 sample: evidence for modified spin-down. The Astrophysical Journal. 913, 1, 70.
4. Beard C., (2024). Leveraging Large, Disparate Datasets to Precisely Measure the Masses of Nearby Exoplanets (Doctoral dissertation, University of California, Irvine).
5. Cloutier R., (2019). The Independent Discovery of Planet Candidates around Low-mass Stars and Astrophysical False Positives from the First Two TESS Sectors. The Astronomical Journal. 158, 2, 81.
6. Messina S., and Guinan E. F., (2002). Magnetic activity of six young solar analogues I. Starspot cycles from long-term photometry. Astronomy and Astrophysics. 393, 1, 225-237.
7. Mascareño A. S., Rebolo R., and Hernández J. G., (2016). Magnetic cycles and rotation periods of late-type stars from photometric time series. Astronomy and Astrophysics 595, A12.
8. Zicher N., Barragán O., Klein B., Aigrain S., Owen J. E., Gandolfi D., and Nicholson B., (2022). One year of AU Mic with HARPS–I. measuring the masses of the two transiting planets. Monthly Notices of the Royal Astronomical Society. 512, 2, 3060-3078.
9. Cauley P. W., Kuckein C., Redfield S., Shkolnik E. L., Denker C., Llama J., and Verma M., (2018). The effects of stellar activity on optical high-resolution exoplanet transmission spectra. The Astronomical Journal. 156, 5, 189.

10. Plavchan P., Vasisht G., Beichman C., Cegla H., Dumusque X., Wang S., and Wright J., (2020). Earth Finder probe mission concept study: characterizing nearby stellar exoplanet systems with earth-mass analogs for future direct imaging. NASA Science.
11. Claytor Z. R., van Saders J. L., Cao L., Pinsonneault M. H., Teske J., and Beaton R. L., (2024). TESS stellar rotation up to 80 days in the southern continuous viewing zone. The Astrophysical Journal. 962, 1, 47.
12. Corsaro E., Bonanno A., Mathur S., García R. A., Santos A. R. G., Breton S. N., and Khalatyan A., (2021). A calibration of the Rossby number from asteroseismology. Astronomy and Astrophysics. 652, L2.
13. Rajpaul V., Aigrain S., Osborne M. A., Reece S., and Roberts S., (2015). A Gaussian process framework for modelling stellar activity signals in radial velocity data. Monthly Notices of the Royal Astronomical Society. 452, 3, 2269-2291.
14. Roettenbacher R. M., Cabot S. H., Fischer D. A., Monnier J. D., Henry G. W., Harmon R. O. and Levine S., (2021). EXPRES. III. Revealing the Stellar Activity Radial Velocity Signature of ϵ Eridani with Photometry and Interferometry. The Astronomical Journal. 163, 1, 19.
15. Salinas H., Pichara K., Brahm R., Pérez-Galarce F., and Mery D., (2023). Distinguishing a planetary transit from false positives: a Transformer-based classification for planetary transit signals. Monthly Notices of the Royal Astronomical Society. 522, 3, 3201-3216.
16. Plotnykov M., and Valencia D., (2024). Observation uncertainty effects on the precision of interior planetary parameters. Monthly Notices of the Royal Astronomical Society. 530, 3, 3488-3499.
17. Bowman D. M., Burssens S., Simón-Díaz S., Edelmann P. V. F., Rogers T. M., Horst L. and Aerts C., (2020). Photometric detection of internal gravity waves in upper main-sequence stars-II. Combined TESS photometry and high-resolution spectroscopy. Astronomy and Astrophysics. 640, A36.
18. Foreman-Mackey D., Luger R., Agol E., Barclay T., Bouma L. G., Brandt T. D., and Savel A. B., (2021). exoplanet: Gradient-based probabilistic inference for exoplanet data and other astronomical time series. arXiv preprint arXiv:2105.01994.
19. Luger R., Agol E., Foreman-Mackey D., Fleming D. P., Lustig-Yaeger J., and Deitrick R. (2019). STARRY: Analytic occultation light curves. The astronomical journal. 157, 2, 64.

20. Yalçınkaya S., Esmer E. M., Baştürk Ö. Z. G. Ü. R., Muhaymin A., Kutluay A. C., Silistre D. İ., and Yeşilyaprak C., (2024). Looking for timing variations in the transits of 16 exoplanets. Monthly Notices of the Royal Astronomical Society. 530, 3, 2475-2495.
21. Nari N., Dumusque X., Hara N. C., Mascareño A. S., Cretignier M., Hernández J. G., and Venturini J., (2025). Revisiting the multi-planetary system of the nearby star HD 20794-Confirmation of a low-mass planet in the habitable zone of a nearby G-dwarf. Astronomy and Astrophysics. 693, A297.
22. Cortés-Zuleta P., Boisse I., Klein B., Martioli E., Cristofari P. I., Antoniadis-Karnavas A., and Udry S., (2023). Optical and near-infrared stellar activity characterization of the early M dwarf Gl 205 with SOPHIE and SPIRou. Astronomy and Astrophysics. 673, A14.
23. Anthony F., Núñez A., Agüeros M. A., Curtis J. L., do Nascimento Jr J. D., Machado J. M., and Wood M. L., (2022). Activity and Rotation of Nearby Field M Dwarfs in the TESS Southern Continuous Viewing Zone. The Astronomical Journal. 163. 6, 257.
24. Claytor Z. R., van Saders J. L., Cao L., Pinsonneault M. H., Teske J., and Beaton R. L., (2024). TESS stellar rotation up to 80 days in the southern continuous viewing zone. The Astrophysical Journal. 962, 1, 47.
25. Kemmer J., Lafarga M., Fuhrmeister B., Shan Y., Schöfer P., Jeffers S. V., and Reffert S., (2025). The CARMENES search for exoplanets around M dwarfs-Cluster analysis of signals from spectral activity indicators to search for shared periods. Astronomy and Astrophysics. 697, A225.